APPENDIX A: ACOUSTIC DOPPLER CURRENTMETER PROFILES (ADCP)

A SHORT HISTORY OF THE MONITORING STATION

In September 2004 a monitoring station, serviced 37 times up to now, was first deployed in the southern channel of the Espartel Sill at ~360m depth (Figure 1). A 75kHz, up-looking RDI Workhorse ADCP (RDI hereinafter) profiled the water column from ~35m above the seafloor until ~50m below the surface where sidelobe interference with the sea surface yields poor measurements (Teledyne, 2011). As an exception, from September 2006 to October 2007 a 150 kHz RDI ADCP was used instead, which provided similar performance, although a slightly shorter range. Sampling interval was set to 30min and bin width reduced from 8m (2004-16) to 6m from March 2016 onwards. Velocity data have been systematically checked for quality, corrected for magnetic declination and rotated 17° counter clockwise to obtain along-strait velocity, which is the component involved in outflow computations.

In September 2016, a new 500kHz Nortek Signature ADCP (Sig-500, hereinafter) was placed down-looking in the mooring line (see inset in Figure A1-a) with the aim of profiling and resolving the deep boundary layer, whose contribution to the outflow is known to be of certain relevance (*Sammartino et al.*, 2015). The instrument profiled 1 m thick bins with a minimum blanking of 0.5m. The ping-to-ping interval was set to 36s and averaging ensembles to 30min in order to match the configuration of the RDI, the main instrument. The objective was to extend the information on the bottom layer dynamics disclosed by the new instrument back in time to the previous dataset in order to improve the accuracy of the historic outflow estimates.

RELEVANT ISSUES OF THE RDI PROFILES

Figure A1-a shows the time-averaged along-strait current from February to December 2019 collected by both ADCPs. The increase of speed in the two-deepest bins of the RDI, marked with asterisks in Figure A1-a, has its origin in the diurnal modulation of the tidal current: the expected decreasing-toward-seafloor profile of velocity is not met one out of every two tidal cycles in these bins (*Sammartino et al.*, 2015). Inspection of the attitude of the instrument, which depends on the response of the lodging buoy to the drag, shows large tilts of the RDI coeval with the increase of the recorded velocity. It results in a drop of instrument accuracy (Figure A1-b) and, hence, in poor velocity estimations. For this reason, recorded values in these bins have been excluded in the outflow computed so far, which has used interpolated values instead.

Interpolation on the other hand is necessary to fill the gap caused by technical and electronic limitations: pulse length and blanking of instruments and the mooring line design leave a vertical window of ~20m thick without data (Figure A1-a). Velocity profile in the bottom boundary layer is logarithmic. To represent this profile, the law-of-wall (LoW, hereinafter, see *Kundu and Cohen* (2004) for instance)

$$U(z) = \frac{u^*}{k} \ln\left(\frac{z}{z_0}\right) \qquad [A.1]$$

is widely accepted. Here, u^* is the friction velocity that depends on the shear stress at the bottom, z_0 is the height above the bottom where velocity is assumed to be zero (roughness length, *Thorpe*, 2007), and k is the dimensionless von Karman's constant, empirically estimated as 0.41. Although the LoW is generally verified in boundary layer dynamics, ocean bottom layers often show deviations and exhibit changes in the rate of decrease few meters above the seafloor. The modified version of the LoW presented in *Perlin et al.* (2005)

$$U(z) = \frac{u^*}{k} \ln\left(\frac{z(h - z_0)}{z_0(h - z)}\right) \qquad [A.2]$$

can account for these changes by introducing a new term h that depends on the Ozmidov scale characteristic of stratified layers (*Thorpe*, 2007). Any of them could be used to fill the gap. *Sammartino et al.* (2015) used the classical LoW [A.1] to infer bottom layer velocities. Near-bottom Sig-500 data were lacking at that time.

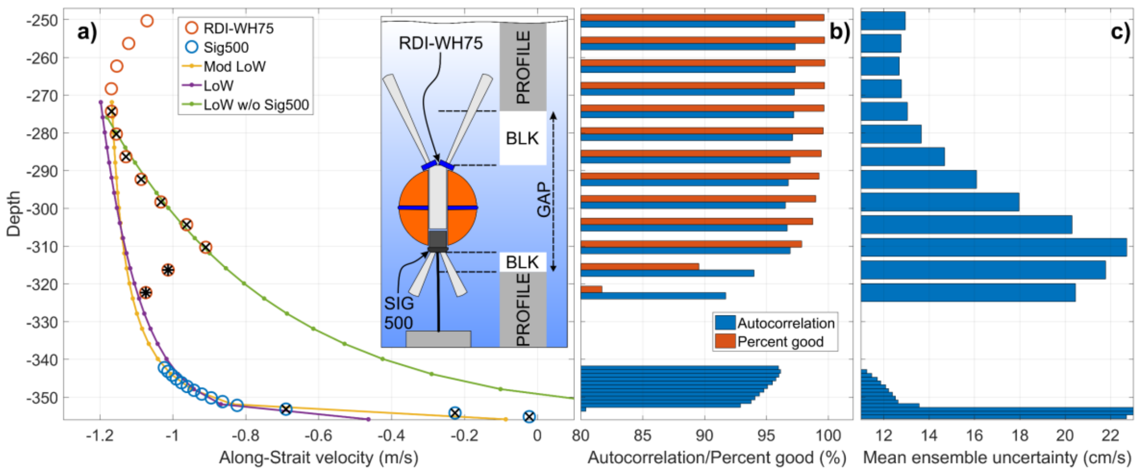

Figure A1.– a) Deepest 100m of the time-averaged profile of along-strait velocity (February to December 2019). RDI profile is in red circles, Sig-500 in blue ones. Rejected RDI bins are marked with asterisks, suspicious bins in both instruments, with crosses. Green line is the LoW fit to RDI data exclusively after excluding the two deepest bins. Purple line is the LoW fit to Sig-500 and RDI data after leaving out the deepest and suspicious bins. Both fits use equation [A.1]. Yellow line is like the purple one but using equation [A.2]. The inset illustrates the origin of the gap. b) Averaged profiles of Autocorrelation for RDI and Sig-500 (light blue) and Percent good for RDI (red), that is, percentage of pings with the four beams participating in the recorded velocity. c) Averaged profiles of standard deviation of the ensembles.

New points have arisen when comparing the data collected by both ADCPs. Even excluding the bins affected by high tilt, RDI and Sig-500 profiles do not match (Figure A1-a). Figure A1-c shows that the uncertainty (standard deviation of the averaged pings in the ensemble) in RDI bins increases progressively from the depth of maximum speed (~270 m) downwards. It may be explained by high-frequency fluctuations of the current, a fact partially supported by the good data quality of the implied bins (marked with crosses in Figure A1-a). Sig-500 profiles, however, show very low uncertainty (less than 14 cm/s, Figure A1-c) and high autocorrelation (over 92%, Figure A1-b) above the fourth bin. In these circumstances, not only the two deepest rejected bins of the RDI but also the next 6-7 overlying them are flagged as suspicious.

Green line in Figure A1-a shows the fitting of the LoW to the RDI profile after removing the two rejected bins. The fit is statistically good, but it provides unrealistic coefficients: u^* is ∼20cm/s, five times higher than previous observations (∼4 cm/s in *Johnson et al.*, (1994) and *Perlin et al.*, (2005)), and the roughness length z_0 is more than 6 m, when it is expected to be of few tens of cm in this energetic region. Since the fitting is determined by the suspicious bins (Figure A1-a), neglecting them and promoting the use of Sig-500 data is a better option. Nevertheless, it is worth-mentioning that, in the instantaneous profiles, the logarithmic fit agrees well with the unused suspicious bins, which relaxes the apparently severe solution of leaving them out. Only when diurnal tidal current accelerates and Sig-500 profiles reproduce correctly the peaks that RDI fails to do (due to the tilt spikes), the fitted profile and the discarded suspicious bins differ.

COMBINED RDI AND SIG-500 VELOCITY PROFILES

The three deepest bins of Sig-500 show low autocorrelations (around 60-70%, out of axis range in Figure A1-b) and uncertainties that double those of the rest of the bins (Figure A1-c). Therefore, they have also been excluded in the fit. Purple and yellow lines in Figure A1-a show the results of fitting data to the LoW (equation [A.1]) and its modified version (equation [A.2]), respectively. Any of them provide very reasonable interpolated values of velocity in the vertical gap and give realistic estimates of u^* (few cm/s) and z_0 (tens of cm). Statistically, however, equation [A.2] performs better than [A.1]: RMSEs are $O(10^{-4}$ m) and $O(10^{-2}$ m) and correlation coefficients 0.99 and 0.94 for each of them, respectively. Moreover, equation [A.2] prescribes a reasonable current speed of ∼9 cm/s at 10 cm above the seafloor, whereas equation [A.1] gives an unrealistic value of ∼50 cm/s (deepest points of purple and yellow lines in Figure A1-a, respectively). The better performance of the equation [A.2] in the mean profiles of Figure A1 also applies to the instantaneous profiles, a result that is particularly satisfactory when the current is stronger. The reason is the presence of h in [A.2], which provides an additional degree of freedom that allows for a better adjustment of the whole lower layer profile.

The before-to-September 2016 profiles, when Sig-500 was not at work, have been recalculated to extrapolate the RDI profiles with equation [A.2] after removing the deepest and suspicious bins and assuming a minimum velocity of 10 cm/s at 10 cm above the seafloor. The final result is a new set of along-strait velocity profiles from the very seafloor to the limit of instrumental range (∼50m depth), which has been eventually extended to the sea surface by linear extrapolation. This extrapolation is not of much concern in this study, which focuses on the lower layer (usually below 150m depth). The recalculated profiles yield a median increase of the westward velocity of ∼17% in the deepest 80 m and a median bias of ∼16 cm/s with regards to the *Sammartino et al.* (2015) profiles. The greatest differences are near the bottom, which diminishes their influence in the re-computed series of the outflow (∼4% increase, see main text).

REFERENCES APPENDIX A

Johnson, G. C., R. G. Lueck, and T. B. Sanford (1994), Stress on the Mediterranean Outflow Plume. Part II: Turbulent dissipation and shear measurements, J. Phys. Oceanogr., 24(10), 2084–2092, doi: 10.1175/1520-0485(1994)024.

Kundu, P. K., and I. M. Cohen (2004), Fluid Mechanics, Elsevier Sci.

Perlin, A., J. N. Moum, J.M. Klymak, M. D. Levine, T. Boyd, and P. M. Kosro (2005), A modified law-of-the-wall applied to oceanic bottom boundary layers, J. Geophys. Res., 110, C10S10, doi:10.1029/2004JC002310.

Sammartino, S., J. Garcıa Lafuente, C. Naranjo, J. C. Sanchez Garrido, R. Sanchez Leal, and A. Sanchez Roman (2015), Ten years of marine current measurements in Espartel Sill, Strait of Gibraltar, J. Geophys. Res. Oceans, 120, 6309–6328, doi:10.1002/2014JC010674.

Teledyne RD Instruments (2011), Acoustic Doppler current profiler principles of operation: A practical primer, Rep. P/N 951-6069-00, 56 pp., San Diego, California.

Thorpe, S. A. (2007), An Introduction to Ocean Turbulence, 240 pp., Cambridge Univ. Press, Cambridge, U. K.